Appl. Phys. B (2004)
DOI: 10.1007/s00340-004-1652-x

Applied Physics B
Lasers and Optics

T. SCHAETZ✉
D. LEIBFRIED
J. CHIAVERINI
M.D. BARRETT
J. BRITTON
B. DEMARCO
W.M. ITANO
J.D. JOST
C. LANGER
D.J. WINELAND

Towards a scalable quantum computer/simulator based on trapped ions

National Institute of Standards and Technology, 325 Broadway, Boulder, CO 80305, USA

Received: 22 June 2004/Revised version: 25 August 2004
Published online: 29 September 2004 •

ABSTRACT We describe the concept and experimental demonstration of the basic building blocks of a scalable quantum computer using trapped-ion qubits. The trap structure is divided into subregions where ion qubits can either be held as memory or subjected to individual rotations and multi-qubit gates in processor zones. Thus, ion qubits can become entangled in one trapping zone, then separated and distributed to separate zones (by switching control-electrode potentials) where subsequent single- and two-ion gates, and/or detection is performed. Recent work using these building blocks includes (1) demonstration of a dense-coding protocol, (2) demonstration of enhanced qubit-detection efficiency using quantum logic, (3) generation of GHZ states and their application to enhanced precision in spectroscopy, and (4) the realization of teleportation with atomic qubits. In the final section an analog quantum computer that could provide a shortcut towards quantum simulations under requirements less demanding than those for a universal quantum computer is also described.

PACS 03.67.Lx; 32.80.Qk

1 Basic architecture

1.1 *Original Cirac/Zoller proposal*

Trapped ions as a processor for quantum information were first proposed by Cirac and Zoller in 1995 [1]. The architecture consists of one string of ions stored in a linear quadrupole trap. Two long-lived electronic levels of each ion are used to implement one quantum bit (qubit), well protected against environmental disturbances. The necessary interactions for gate manipulations can be precisely switched on and off by focussed laser beams addressing the qubits individually. To provide a universal set of gates (to be able to implement any algorithm), one needs single-qubit gates and a conditional two-qubit gate. Single-qubit gates are performed with laser pulses exciting resonant transitions between the internal levels of the qubit in question. Two-qubit gates use one normal mode of collective vibration of the ions as a data bus between qubits, i.e. as a means to couple the possibly non-neighboring partners in the gate operation [1]. To this end, all normal modes of vibration have to be precisely initialized, i.e. should be cooled close to the ground state before the algorithm starts.

This proposal stimulated a new field in trapped-ion research, but it soon became clear that it would be difficult to scale the original architecture to several hundred qubits – the amount necessary to perform quantum calculations beyond the capabilities of classical computers. In addition, to implement the probably inevitable error correction, one has to take auxiliary qubits (ancillae) into account. Depending on the error rate, this overhead of approximately 100 ancillae per physical qubit (to provide one fault-tolerant logical qubit) boosts the number to aim for towards 10^5 ions [2].

In particular, confining a linear string of 'only' thousands of ions in one trap would lead to unrealistically high potentials on the end-cap electrodes to counteract their Coulomb repulsion. Keeping the distance between neighboring ions above the diffraction limit of the (individually) addressing laser beam requires rather low axial potentials and therefore decreasing motional frequencies for an increasing number of ions. Low motional frequency and therefore a slow data bus limits gate speeds for the computation (in the original proposal, the gate rate has to be below the lowest motional frequency). Finally, from a practical point of view, the emergence of $3N$ normal modes for N ions plus their sum and difference frequencies leads to an increasingly crowded excitation spectrum where individual components are difficult to identify and off-resonant coupling to 'spectator' transitions is hard to avoid.

1.2 *Multiplexed trap proposal*

In 1998 the group at NIST proposed a multiplexed trap architecture [3, 4] that might alleviate the problems described above and is modular, so scaling to higher qubit numbers seems to be feasible. The basic idea is to expand the original architecture to an array of many independently controllable subtraps (see Fig. 1).

Qubits that do not partake in a given step of the algorithm are stored in 'memory' regions. To execute a gate on certain qubits, they are separated out of the memory regions and shifted into one of the 'processor' regions. Moving ion

✉ Fax: +49-89-32905-336, E-mail: tschaetz@mpq.mpg.de
Present address: Max-Planck-Institut für Quantenoptik (MPQ), Hans-Kopfermann-Str. 1, 85748 Garching, Germany

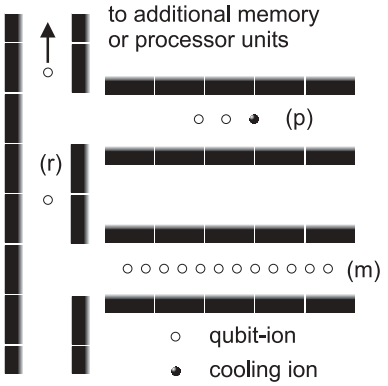

FIGURE 1 Multiplexed trap architecture. An array of independently controllable subtraps holds the ion qubits (the radio-frequency electrodes providing the radial confinement are not displayed). Qubits that are not involved in a given step are held in a 'memory' region (m). Before performing a gate on a certain pair of qubits, they are shifted into a 'processor' unit (p), and sympathetically recooled with another ion species. Single-bit rotations or ancilla read outs can be performed in any region sufficiently isolated from the remaining qubits (for example in (r))

qubits around does not lead to decoherence in the computational Hilbert space spanned by the qubits, since the motion is only used for coupling the qubits during the gate operation in the processor trap. Still, the ion qubits may gain some excess motional energy, but they can be sympathetically recooled close to the ground state with another 'refrigerator' ion [5, 6] before the next gate is applied. Since this cooling overcomes the motional heating, the time available for a computation would be limited only by the decoherence of the internal qubit states. The radiative lifetime of the hyperfine ground states is extremely long (many years). Therefore, the memory decoherence is primarily due to phase errors induced by external perturbations, e.g. magnetic field fluctuations. In a carefully controlled environment, decoherence time scales could be on the order of many days with experimentally demonstrated lower limits of several minutes (see e.g. [7]). A further advantage of the multiplexed architecture is the ability to read out a qubit without compromising neighboring ion qubits through rescattered photons. These read outs can be performed in areas that are sufficiently spatially isolated from the remaining qubits.

All steps described above can be done in a highly parallel fashion, an important prerequisite for efficient error correction. Scaling to many, possibly thousands of, ions is technically challenging, but seems possible without fundamental limitations.

2 Experiments at NIST

The qubits used at NIST are spanned by the $|F = 2, M_F = -2\rangle$ and $|F = 1, M_F = -1\rangle$ ground-state hyperfine levels of $^9Be^+$ labeled $|\downarrow\rangle$ and $|\uparrow\rangle$, respectively (splitting $\omega_0/2\pi = (E_\uparrow - E_\downarrow)/h \simeq 1.25\,\mathrm{GHz}$). In the following, we use the formal equivalence between a two-level system and a spin-$\frac{1}{2}$ magnetic moment in a magnetic field (Bloch-vector representation) [8, 9].

Controlled ion-qubit shuttling is accomplished with negligible heating. Ion separation is accomplished with no detected failures and small heating (about 10 quanta).

To implement quantum information processing (QIP) protocols, we have to realize single-qubit gates (rotations) and two-qubit conditional logic gates [2].

2.1 *Single-qubit gates*

For a single-qubit gate on ion i, the states $|\downarrow\rangle_i$ and $|\uparrow\rangle_i$ are coupled with two-photon stimulated-Raman transitions excited with two laser beams (designated 'blue' and 'red' to indicate their relative detuning) [3]. By tuning the difference frequency of the laser beams to $(\omega_{\mathrm{blue}} - \omega_{\mathrm{red}})/2\pi = \omega_0/2\pi$, we implement rotations of the qubit state on the Bloch sphere

$$R_i(\theta, \phi_i) \equiv \begin{pmatrix} \cos\frac{\theta}{2} & -\mathrm{i}\mathrm{e}^{-\mathrm{i}\phi_i}\sin\frac{\theta}{2} \\ -\mathrm{i}\mathrm{e}^{+\mathrm{i}\phi_i}\sin\frac{\theta}{2} & \cos\frac{\theta}{2} \end{pmatrix}, \qquad (1)$$

where we use the conventions $|\downarrow\rangle \equiv (0, 1)^{\mathrm{T}}$, $|\uparrow\rangle \equiv (1, 0)^{\mathrm{T}}$.

The angle θ is proportional to the duration of the Raman pulse. The phase factor $\phi_i = \Delta\boldsymbol{k}\cdot\boldsymbol{x}_i + \phi_{\mathrm{blue},i} - \phi_{\mathrm{red},i}$ is the phase difference between the Raman beams at the position $\boldsymbol{x}_i$ of the ith ion ($\Delta\boldsymbol{k} \equiv \boldsymbol{k}_{\mathrm{blue}} - \boldsymbol{k}_{\mathrm{red}}$, the wave-vector difference of the Raman beams). There are two different beam geometries used. (a) The beams are oriented such that $\boldsymbol{k}_{\mathrm{blue}}$ is parallel to $\boldsymbol{k}_{\mathrm{red}}(|\Delta\boldsymbol{k}| \simeq 0)$. Motion does not affect the transitions driven by these beams. (b) The $\boldsymbol{k}$ vectors of the beams are oriented such that $\boldsymbol{k}_{\mathrm{blue}}$ is approximately perpendicular to $\boldsymbol{k}_{\mathrm{red}}$ and $\Delta\boldsymbol{k} \equiv \boldsymbol{k}_{\mathrm{blue}} - \boldsymbol{k}_{\mathrm{red}} \simeq \sqrt{2}|\boldsymbol{k}_{\mathrm{blue}}|\hat{z} \equiv \hat{z}2\pi/\lambda_{\mathrm{eff}}$, where λ_{eff} is the effective wavelength of the Raman transition and $\hat{z}$ denotes the direction of the trap axis. These transitions depend sensitively on the ion motion and can therefore be used for cooling and gates where the motion acts as a bus between different qubits.

We will need to implement single-qubit rotations on one ion without changing the state of the neighboring ion; this can be accomplished in one trap zone even though the Raman beams overlap the ions [10].

If we use the intensity profile of the parallel Raman beams (a) to locate the two qubits at different beam intensities, we can rotate one state by e.g. $\theta = 4\pi$, effectively not changing its state, while rotating its neighbor by $\theta = 3\pi$, effectively performing an individual $R_i(\pi, \phi)$ pulse on the second ion.

We can also use the phase of the effective wave provided by the interfering perpendicular beams (b). To see how this is done, consider the following example on two qubits [11]. Suppose we want to prepare the state $(|\downarrow\rangle_1 + |\uparrow\rangle_1) \otimes |\downarrow\rangle_2$ from the state $|\downarrow\rangle_1|\downarrow\rangle_2$ (suppressing state-normalizing factors). We first apply a Raman pulse acting equally on both ions $(R_1(\frac{\pi}{4}, -\frac{\pi}{2}) \otimes R_2(\frac{\pi}{4}, -\frac{\pi}{2}))$. The spins rotate into a state represented pictorially by $|\searrow\rangle_1|\searrow\rangle_2$. The spacing of the ions is now changed by $\lambda_{\mathrm{eff}}/2$. A second Raman pulse of the same duration is applied to both qubits $(R_1(\frac{\pi}{4}, -\frac{\pi}{2}) \otimes R_2(\frac{\pi}{4}, +\frac{\pi}{2}))$ such that the laser phase on qubit 1 is the same but, because of the change in ion separation, the phase on qubit 2 is shifted by π. Thus, qubit 2 is rotated back into its initial state while qubit 1 completes a $\theta = \frac{\pi}{2}$ rotation. Pictorially, application of the second Raman pulse implements the transformation $|\searrow\rangle_1|\searrow\rangle_2 \rightarrow |\rightarrow\rangle_1|\downarrow\rangle_2 = (|\downarrow\rangle_1 + |\uparrow\rangle_1) \otimes |\downarrow\rangle_2$.

Generalizing this, we can apply the Pauli operators σ_x, σ_y, and σ_z to ion 1, which, up to global phase factors, correspond to the operators $R_1(\pi, 0)$, $R_1(\pi, \frac{\pi}{2})$, and $R_1(\pi, 0)R_1(\pi, \frac{\pi}{2})$, respectively.

2.2 *Conditional two-qubit gates*

To implement universal logic between the ions, the Raman laser beams can be configured to apply state-dependent optical dipole forces. We choose the polarizations of the beams so that these forces along the z direction are related by $\boldsymbol{F}_{\downarrow} = -2\boldsymbol{F}_{\uparrow}$ [12, 13]. We implemented different versions of this gate on two or three ions using different normal modes as data bus. We describe here a two-qubit gate using the stretch (breathing) mode to elucidate the basic idea. We adjust the frequency difference between the Raman beams and therefore the frequency of the optical dipole force to be equal to $\omega_{\mathrm{STR}} + \delta$ ($|\delta| \ll \omega_{\mathrm{STR}}$). The ions are separated by a distance $m \times \lambda_{\mathrm{eff}}$ (were m is an integer). By applying the state-dependent dipole forces for a gate time $\tau_{\mathrm{G}} = 2\pi/\delta$ and adjusting their magnitude appropriately, we coherently excite the motion of two ion qubits along a closed path in motional phase space if they are in different internal states, while they are not excited if they are in the same state. The different state combinations of the ions pick up a phase proportional to the phase-space area circumscribed, leading to a geometric phase gate G_{ϕ}, which implements the operation [12]

$$\begin{aligned} G_{\phi}:\ & a|\downarrow\rangle|\downarrow\rangle + b|\downarrow\rangle|\uparrow\rangle + c|\uparrow\rangle|\downarrow\rangle + d|\uparrow\rangle|\uparrow\rangle \\ & \rightarrow a|\downarrow\rangle|\downarrow\rangle + \mathrm{e}^{\mathrm{i}\phi} b|\downarrow\rangle|\uparrow\rangle + \mathrm{e}^{\mathrm{i}\phi} c|\uparrow\rangle|\downarrow\rangle + d|\uparrow\rangle|\uparrow\rangle\,. \end{aligned} \tag{2}$$

The gate can be converted into a π-phase gate or a controlled NOT (CNOT) gate with single-bit rotations for $\phi = \pi/2$. Starting, for example, with the state $|\downarrow\downarrow\rangle$ and sandwiching this gate between $\pi/2$ and $3\pi/2$ (spin-echo) pulses applied to both ions, we are able to produce maximally entangled states of the form $|\psi\rangle = |\downarrow\downarrow\rangle + |\uparrow\uparrow\rangle$ [14] with a fidelity of 0.97 [12].

2.3 *State-sensitive detection*

We distinguish the two states of a qubit, $|\downarrow\rangle$ and $|\uparrow\rangle$, by observing state-dependent laser-driven fluorescence. The laser-beam frequency is tuned to drive the qubit from the $|\downarrow\rangle$ state to some excited state, which subsequently decays back to $|\downarrow\rangle$, emitting a photon that can be detected. When the the qubit is in the $|\uparrow\rangle$ state, laser-beam scattering is absent and, for the $|\downarrow\rangle$ state, the qubit scatters many photons [15].

2.4 *Sources of error*

In practice, the largest contribution to errors is due to fluctuations of the magnetic field. However, we employ the technique of spin echoes [9] to correct the related dephasing. Aside from adding global phase factors, the spin-echo pulses do not change the protocols and are omitted in the following discussions. Remaining errors are due to fluctuations in the trap frequency, fluctuations in the Raman-beam intensity, and spontaneous emission during the gate operation. If frequency drift and intensity errors could be reduced to order 10^{-3} and spontaneous emission suppressed (i.e. by using a different ion species [13]), the expected gate fidelity is on the order of 0.9999.

3 Demonstration experiments

On the way towards scalable quantum computation in the multiplexed architecture, we can perform experiments involving the basic elements of QIP while testing the viability of the tools described above and required for large-scale processing [3, 11], including the capability for (1) separation and transfer of qubits between traps while maintaining their entanglement, (2) individual addressing (in tight confinement), (3) single- and two-qubit gates, (4) using decoherence-free subspaces [11], (5) using measurement outcomes of ancilla qubits to trigger conditional operations, and (6) implementing nonlocal operations.

In addition, the implementation of experimental protocols serves as a benchmark for comparison of QIP in different physical realizations [16].

For the experiments described below, we typically adjust the axial trap potential to make the lowest normal mode frequency $\omega_{\mathrm{COM}}/2\pi \approx 4$ MHz, corresponding to an inter-ion separation of approximately 4 μm. At the start of each experiment, the ions are laser cooled to the motional ground state and optically pumped into the internal states $|\downarrow\rangle \ldots |\downarrow\rangle$ [17].

3.1 *Quantum dense coding* [19]

Quantum dense coding was first proposed by Bennett and Wiesner in 1992 [19]. Their scheme enables the communication of two bits of classical information (00, 01, 10, 11) with the transmission of one qubit. Initially, two parties, called Alice and Bob, each hold one qubit of a maximally entangled pair [14]. Bob applies one of four possible unitary operations (each identified with one state of two classical bits shown above) to his qubit. Due to the shared entanglement, the two qubits cannot be described individually and Bob's operation affects both, even though they are spatially separated. Bob then sends his qubit to Alice. She performs a Bell measurement [20] of both qubits. One of the four possible outcomes in the measurement basis ($|\downarrow\downarrow\rangle$, $|\downarrow\uparrow\rangle$, $|\uparrow\downarrow\rangle$, and $|\uparrow\uparrow\rangle$) tells her which of the four operations Bob applied and the corresponding two-bit classical number.

Parts of this protocol were first demonstrated in optics, where the qubit states were represented by a photon's states of polarization [21]. A drawback was, and still is, that two of the Bell states cannot be distinguished; thus, only three different measurement outcomes are possible (called a 'trit' of information). The experiment with photons also requires post-selection and many entangled photon pairs are necessary to realize the transmission of one 'trit'.

In our implementation [18], a pair of entangled qubits is prepared by the phase gate described in Sect. 2.2. We let Bob use the experimental apparatus first to encode his qubit. He applies a single-qubit rotation, σ_x, σ_y, σ_z, or no rotation (identity $\tilde{I}$), correlated with his message to be transferred. He then turns over the apparatus to Alice so that she can decode the message by applying a Bell measurement [20] using Bob's and her qubits.

For each choice of Bob's operator, we measure the fidelity of the actual output state relative to the ideally expected one. This data is included (in bold lettering) in Table 1, where we also display the probabilities for detecting all other (undesired) states.

	$\tilde{I}$	σ_y	σ_z	σ_x
$\|\downarrow\rangle_B\|\downarrow\rangle_A$	**0.84(2)**	0.07(1)	0.08(1)	0.02(1)
$\|\uparrow\rangle_B\|\downarrow\rangle_A$	0.07(1)	0.01(1)	**0.84(1)**	0.04(1)
$\|\downarrow\rangle_B\|\uparrow\rangle_A$	0.06(1)	**0.84(1)**	0.04(1)	0.08(1)
$\|\uparrow\rangle_B\|\uparrow\rangle_A$	0.03(1)	0.08(1)	0.04(1)	**0.87(1)**

TABLE 1 Correlations between Bob's applied operator (*top row*) and Alice's state measurements of both qubits (*left-hand column*). The entries correspond to the probabilities measured by Alice for each basis state. Ideally, the entries *in bold* should equal 1 and all other entries should equal 0

To summarize, we implement the basic protocol [19], without the need for post-selection of data, and with the ability to transfer and detect all four Bell states corresponding to Bob's two bits of classical information with an average fidelity of 0.85(1). In spite of experimental imperfections, the information transferred exceeds what is possible by transferring one classical bit.

3.2 *Enhancement of detection efficiency by QIP* [23]

If the coherent operations (gates) used in an algorithm can be performed with higher efficiency than the state detection (read out), the overall efficiency is restricted by the latter. Therefore, low single bit detection efficiency F_{det} could be the bottleneck for scalable quantum computation.

With low detection efficiency, it may require excessive repetition of an algorithm in order to reliably determine its output. This is undesirable for algorithms involving many gates followed by a single measurement. Also, if the algorithm requires a significant amount of error correction, detection errors are compounded and repetition may fail to give the desired result. The read out of a projected state of N qubits, as in Shor's factoring algorithm, leads to an overall read-out fidelity F_{det}^{N} that decreases exponentially with N, i.e. requires an exponentially large number of measurements and repetitions of the algorithm to determine a useful output.

Low detection efficiency can render a system unscalable because the required maximum tolerable error rate is not achieved for all operations including detection. Finally, even if scalability is within reach, the failure of measurements needed for error correction during the computation requires additional overhead to avoid miscorrecting errors.

Improving state detection without repetition of the algorithm would be an easy task if one could copy the final state to be measured. This is precluded by the impossibility of cloning a general quantum state [2]. However, a way to enhance state-detection fidelity by using quantum logic gates in conjunction with auxiliary 'ancilla' qubits is outlined in [23]. For simplicity, consider a qubit in the superposition state $|\psi\rangle = \alpha_0|0\rangle + \alpha_1|1\rangle$. A sequence of M CNOT gates [2] involving ancillae a1, a2, ... , aM reserved for this qubit encodes $|\psi\rangle$ to an entangled state according to the transformation

$$\begin{aligned}&\big(\alpha_0|0\rangle+\alpha_1|1\rangle\big)|0\rangle_{a1}|0\rangle_{a2}\ldots|0\rangle_{aM}\\ &\longrightarrow \alpha_0|0\rangle|0\rangle_{a1}|0\rangle_{a2}\ldots|0\rangle_{aM}+\alpha_1|1\rangle|1\rangle_{a1}|1\rangle_{a2}\ldots|1\rangle_{aM}\,. \quad (3)\end{aligned}$$

Effectively, we amplify the input state to get $M+1$ tries to determine which state each qubit is projected into. We can then use a majority vote to determine the correct read out, therefore reducing the measurement uncertainty in the detection process [23].

We have implemented this general protocol using atomic qubits. For one qubit, to distinguish the two states $|\downarrow\rangle$ and $|\uparrow\rangle$, we use the number of detected photons n_{det} obtained by state-dependent fluorescence detection (see Sect. 2.3). First, we have to define a threshold n_1 (which depends on the duration of the detection). If $n_{\mathrm{det}} > n_1$, the state is read out as $|\downarrow\rangle$; if $n_{\mathrm{det}} \le n_1$, the state is read out as $|\uparrow\rangle$ (see Fig. 2). If the detected counts in one measurement happen to be where the distributions $\mathrm{D}_\uparrow$ for $|\uparrow\rangle$ and $\mathrm{D}_\downarrow$ for $|\downarrow\rangle$ overlap, the state assignment is ambiguous. In general, the optimum value of n_1 is determined by minimizing simultaneously the fractions of $\mathrm{D}_\uparrow$ with $n_{\mathrm{det}} > n_1$ and $\mathrm{D}_\downarrow$ with $n_{\mathrm{det}} \le n_1$. The average error is determined by the normalized sum of the experiments in the $\mathrm{D}_\uparrow$-histogram for $n_{\mathrm{det}} > n_1$ and the $\mathrm{D}_\downarrow$-histogram for $n_{\mathrm{det}} \le n_1$. Importantly, the overlap, and therefore the average error, is much smaller for two qubits in the same state $|\downarrow\rangle|\downarrow\rangle$ with distribution $\mathrm{D}_{\downarrow\downarrow}$ or $|\uparrow\rangle|\uparrow\rangle$ with distribution $\mathrm{D}_{\uparrow\uparrow}$ and the decision threshold n_2 is determined in the same manner as n_1.

In our experiment [22], we have low background noise ($\langle\dot{n}_{\mathrm{bkg}}\rangle \ll \langle\dot{n}_\downarrow\rangle$, where $\langle\dot{n}_\downarrow\rangle = \frac{1}{2}\langle\dot{n}_{\downarrow\downarrow}\rangle = 2.5\times10^4\,\mathrm{s}^{-1}$ is the count rate for the $|\downarrow\rangle$ state), and the detection efficiency is high, at least compared to the gate fidelities that are typically achieved. Therefore, to investigate the fundamental features of the enhancement scheme, we add Poissonian count noise to the detected ion fluorescence. We then increase our detection efficiency using one ancilla qubit initialized, for experimental convenience, in a superposition state. Using the effective individual addressing technique described in Sect. 2.1, the generic initial state of the two qubits is $\Psi_{\mathrm{initial}} = (\alpha_\downarrow|\downarrow\rangle +$

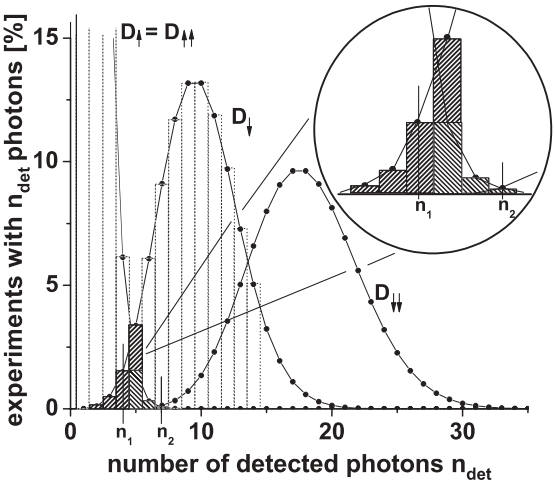

FIGURE 2 Simulated Poissonian distributions D of photon counts for the detection of fluorescence in the case of (*left* to *right*) zero, one, or two qubits in the $|\downarrow\rangle$ state (the state that scatters photons). Background noise counts are responsible for the finite photon counts in $\mathrm{D}_\uparrow$. For the plot shown, the rate of background noise counts $\langle\dot{n}_{\mathrm{bkg}}\rangle = 0.125\langle\dot{n}_\downarrow\rangle$ and the detection duration is taken to be 324 μs (chosen to correspond to the actual experiment). The state determination is ambiguous for detected counts n_{det} where the $\mathrm{D}_\uparrow$ and the $\mathrm{D}_\downarrow$ distributions overlap (see *magnified inset*), leading to errors. Two qubits being either in the $|\downarrow\rangle|\downarrow\rangle$ state with distribution $\mathrm{D}_{\downarrow\downarrow}$ or in the $|\uparrow\rangle|\uparrow\rangle$ state with distribution $\mathrm{D}_{\uparrow\uparrow}$ provide a smaller overlap of the distributions, and thus a smaller read-out error

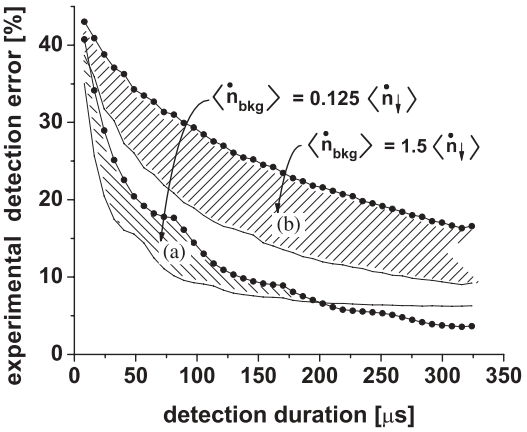

FIGURE 3 Experimental error in state identification as a function of the detection duration at a given average count rate $\langle \dot{n}_\downarrow \rangle = 2.5 \times 10^4\ \mathrm{s}^{-1}$, for two levels of background noise. The one-qubit cases (without encoding) are represented by the *dotted lines* and the one-ancilla encoded case by the *solid lines*, respectively. The *shaded areas* emphasize the reduction of the error by the encoded detection scheme. To emphasize the results in the case of background noise, we add a background count rate of $\langle \dot{n}_{\mathrm{bkg}} \rangle = 0.125 \langle \dot{n}_\downarrow \rangle$ (a) and of $\langle \dot{n}_{\mathrm{bkg}} \rangle = 1.5 \langle \dot{n}_\downarrow \rangle$ (b). Since the photon-number thresholds (see Fig. 1) are integers, the curves can show steps where n_1 and n_2 change

$\alpha_\uparrow|\uparrow\rangle)(|\downarrow\rangle_\mathrm{a} + |\uparrow\rangle_\mathrm{a})$. We implement the operation

$$\Psi_{\mathrm{initial}} \rightarrow R_\mathrm{a}\left(\frac{\pi}{2}, \frac{\pi}{2}\right) G_{\pi/2}\Psi_{\mathrm{initial}} = \alpha_\downarrow|\downarrow\rangle|\downarrow\rangle_\mathrm{a} + \alpha_\uparrow|\uparrow\rangle|\uparrow\rangle_\mathrm{a}\,. \tag{4}$$

We then measure the fluorescence from both qubits, since the measurement projects this general input state to either $|\downarrow\downarrow\rangle$ with probability $|\alpha_\downarrow|^2$ or $|\uparrow\uparrow\rangle$ with probability $|\alpha_\uparrow|^2$. To analyze the gain of this protocol it is sufficient to produce two different input cases: (1) $\alpha_\downarrow = 1$ and (2) $\alpha_\uparrow = 1$. As shown in Fig. 3, the histogram overlaps and corresponding detection errors decrease as the detection duration increases (except for case (a) beyond 200 μs).

The shaded areas emphasize the reduction of the error by the encoded detection scheme. The differences between theoretically achievable and the observed results are primarily due to the infidelity in the experimental gates.

To achieve fault tolerance in the future, the fidelity of coherent operations will have to be close to 1. Thus, in the case where a lengthy quantum algorithm is limited by comparably poor detection efficiency, a method like the one described here is advantageous. The improvement in detection efficiency would be even more significant, and can be amplified to be as high as the fidelity of the gate operations, as more ancilla qubits are used.

3.3 *Three-qubit entanglement and spectroscopy beyond the standard quantum limit* [25]

Entanglement between qubits can be used to beat the statistical limitations in spectroscopic precision [25] of uncorrelated particles. Ultimately the fundamental precision limit, governed by the Heisenberg uncertainty principle, can be reached. To show how this is done, we can compare one of the most basic spectroscopic measurements, a Ramsey experiment on independent qubits, with one on qubits sharing entanglement.

To perform a Ramsey experiment on one qubit, a first Ramsey pulse $R(\frac{\pi}{2}, 0)$ at frequency ω (here $\omega \neq \omega_0$) is applied, rotating the state $|\downarrow\rangle$ represented on the Bloch sphere into the horizontal plane. A free precession for the duration t evolves the phase ϕ (in the frame co-rotating at the resonant frequency ω_0 of the two-level system) to $\phi = (\omega - \omega_0)t$. Since a simple state detection would be insensitive to this phase, a second Ramsey pulse $R(\frac{\pi}{2}, 0)$ translates the phase information into the measurement basis. By measuring the state population after this pulse sequence, we obtain oscillations between the two eigenstates, $|\downarrow\rangle$ and $|\uparrow\rangle$, depending on the accumulated phase ϕ. We have $P_\downarrow = 1/2(1 - \cos[\omega - \omega_0]t) = 1 - P_\uparrow$. These fringes allow for the determination of ω_0. To increase the spectroscopic resolution, one can either increase the precession time t or equivalently the number of qubits. An increase to N qubits will provide an ensemble of N independent qubits in superposition states after the first Ramsey pulse $R_1 \otimes \cdots \otimes R_N$ (see Fig. 4a). This leads to a maximum gain in spectroscopic resolution proportional to $\sqrt{N}$, due to the statistical limit [26], equivalent to repeating the measurement N times on one qubit. Replacing the first Ramsey pulse by an operation that produces the entangled state $\Psi = |\downarrow\downarrow\downarrow \ldots \downarrow\rangle + |\uparrow\uparrow\uparrow \ldots \uparrow\rangle$ would be equivalent to creating a 'superatom' at $t = 0$ (see Fig. 4b), where the energy difference between the two new states of the superposition is N times larger than in the non-entangled individual cases. In a spectroscopic measurement, this corresponds to a gain in resolution proportional to N, the Heisenberg limit. Thus, a gain in precision by a factor of $\sqrt{N}$ can be achieved over the best possible spectroscopy with non-entangled states.

For three qubits, this superatom state $\Psi = |\downarrow\downarrow\downarrow\rangle + |\uparrow\uparrow\uparrow\rangle$ is called a GHZ state [27] and can be provided by an entangling gate operation like the one described in Sect. 2.2, except that the coherent drive uses the Center-of-mass (COM)-mode frequency of three-qubit ions [24]. Embedding the gate drive in the first arm of a spin-echo experiment can be viewed as the first Ramsey pulse described above creating the entangled 'superatom' of three qubits. After the free-precession duration t the state evolves to $\Psi = |\downarrow\downarrow\downarrow\rangle + \mathrm{e}^{-\mathrm{i}3\omega_0 t}|\uparrow\uparrow\uparrow\rangle$ (here equivalently replaced by a variable phase change of the following pulse). We then apply the equivalent of the second Ramsey pulse by repeating the same pulse sequence. The read-out measurement projects the state to either $|\downarrow\downarrow\downarrow\rangle$ with probability $P_{\downarrow\downarrow\downarrow} = 1/2(1 - \cos[3\phi])$ or $|\uparrow\uparrow\uparrow\rangle$ with probabil-

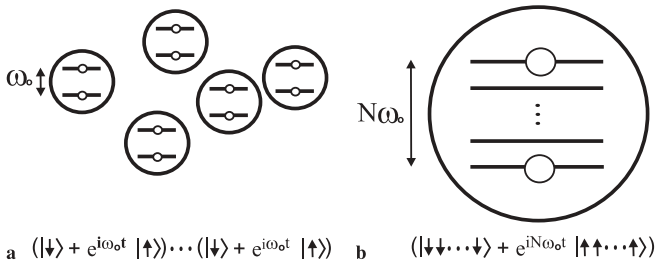

FIGURE 4 Applying a Ramsey pulse to N qubits creates a superposition state. For N independent qubits (**a**) it creates a product state of qubits in independent superposition states. The entangled state of N qubits is shown in (**b**), where the energy difference between the two states of the 'superatom' is N times higher, providing $\sqrt{N}$ higher resolution in a spectroscopic measurement for a duration t of free precession t between two Ramsey pulses

ity $P_{\uparrow\uparrow\uparrow} = 1 - P_{\downarrow\downarrow\downarrow}$. The two outcomes are optimally immune against read-out errors due to the minimal overlap of the photon distributions for the two outcome possibilities (see Fig. 2 for the corresponding two-qubit case).

In our experiment [24], the measured fidelity for the preparation of the GHZ state was 0.89(3). Using this state leads to a gain in spectroscopic resolution by a factor of 1.45(2) compared to a perfect Ramsey experiment with non-entangled qubits. The gain for a Heisenberg-limited measurement of a factor of $\sqrt{3} = 1.78$ $\left(\sqrt{N}\right)$ is reduced due to imperfect gate operations and read out.

Since only collective ensemble preparation and detection pulses are used, the extension of the method to larger numbers of qubits is straightforward.

3.4 *Quantum teleportation* [29]

Quantum teleportation [29] realizes the transfer of quantum information from one location to another without the physical transfer of the associated quantum information carrier. The non-local correlations of spatially separated but entangled qubits are used, as in the dense-coding protocol described in Sect. 3.1, but the necessary information to complete the teleportation is transmitted via a classical channel.

Bob wants to teleport the superposition spin state of a qubit (labeled T) to Alice. The state can be described by the wave function $|\Psi\rangle_{\mathrm{T}} \equiv \alpha_{\uparrow}|\uparrow\rangle_{\mathrm{T}} + \alpha_{\downarrow}|\downarrow\rangle_{\mathrm{T}}$ and could even be unknown (to him or anybody else). In addition, Alice and Bob hold one qubit of a two-qubit entangled pair [14] that we assume to be described by the singlet $|S\rangle_{\mathrm{A,B}} \equiv |\downarrow\rangle_{\mathrm{A}}|\uparrow\rangle_{\mathrm{B}} - |\uparrow\rangle_{\mathrm{A}}|\downarrow\rangle_{\mathrm{B}}$. Thus, Bob possesses qubits B and T, while Alice holds qubit A. Bob can transfer the state of qubit T to Alice using only classical information about the outcome of a Bell measurement [20] he performs on qubits B and T. For the case of a qubit, two bits of classical information are necessary even though the precise description of a general qubit would require an infinite amount of classical information. Once Alice receives this classical information, she can perform a conditional operation on her qubit A, turning it exactly into qubit T. No cloning of qubit T occurred, since the state of this qubit is completely erased after the Bell measurement. Also, 'faster than light communication' did not occur, because of the limited speed for the transfer of the necessary classical information.

In the experiment [28], we initialize the three qubits to the state $|\downarrow\downarrow\downarrow\rangle_{\mathrm{A,T,B}}$. We apply the phase gate described in Sect. 2.2 on the stretch mode of the three qubits. Since the amplitude of motion for the middle qubit T is zero, the entanglement pulse on the three qubits has no effect on qubit T and produces the state $(|\downarrow\downarrow\rangle_{\mathrm{A,B}} + |\uparrow\uparrow\rangle_{\mathrm{A,B}}) \otimes |\downarrow\rangle_{\mathrm{T}}$. Using the effective individual addressing techniques described in Sect. 2.1, we transform qubits A and B into the singlet state while leaving qubit T unaffected $((|\downarrow\uparrow\rangle_{\mathrm{A,B}} - |\uparrow\downarrow\rangle_{\mathrm{A,B}}) \otimes |\downarrow\rangle_{\mathrm{T}})$. The singlet state, being immune to global rotations [11], allows for a single-qubit rotation applied to all three qubits, but effectively only addresses qubit T and transforms it into the input state to be teleported. Separating qubit A to a different trapping zone with a distance of 300 μm from the zone containing B and T provides the possibility to perform a Bell measurement on qubits B and T only [20]. The outcome of this measurement, one out of four possibilities, is the classical information needed to apply one of the four possible operations on qubit A to finish the teleportation and rotate the state of qubit A into the one T was in originally.

To determine the average fidelity of the complete protocol, we first teleport $|\downarrow\rangle_{\mathrm{T}}$ and $|\uparrow\rangle_{\mathrm{T}}$ and achieve a fidelity of about 80%. We then perform a one-qubit Ramsey experiment[1], where the first Ramsey pulse is applied to qubit T (the one to be teleported). The Ramsey protocol is completed with the second pulse applied to Alice's qubit A after the teleportation. The Ramsey fringes obtained for two different relative phases between the two Ramsey pulses, together with the $|\downarrow\rangle_{\mathrm{T}}$ and $|\uparrow\rangle_{\mathrm{T}}$ cases, yield the average teleportation fidelity $\langle F\rangle = 78 \pm 2\%$, achieved on demand without post-selection of data.

3.5 *Sympathetic recooling*

Sympathetic recooling is a crucial step to extend the capability of QIP with trapped ions to time scales much longer than the time constant for motional heating (acquired due to separation, shuttling, or other heating mechanisms in the trap [33]). It must recool the ions sufficiently close to the motional ground state so that the fidelity of subsequent quantum gates is not affected.

Sympathetic cooling has previously been demonstrated using 'refrigerator' ions that are the same as the qubit ions [30] or an isotope of the qubit ions [6]. In order to gain higher immunity from decoherence caused by (stray) cooling light, we have chosen a different ion species for the refrigerator ion. The cooling laser can be far detuned from all qubit transitions; therefore, individual addressing is not required.

We stored and Doppler cooled one $^{9}Be^{+}$ ion and one $^{24}Mg^{+}$ ion in the same trap. We then cooled either the Mg^{+} ion or the Be^{+} ion close to the ground state [5]. When cooling the Mg^{+} ion we were technically limited by our Raman detuning and achieved $\bar{n} = 0.19(6)$ and $\bar{n} = 0.52(7)$ for the two normal modes, respectively. This result will be improved in the future by implementing higher Raman detuning. Cooling the two ions through the Be^{+} ion (where the detuning is large) yielded limits of $\bar{n} = 0.03(2)$ and $\bar{n} = 0.04(3)$.

For trapped-ion QIP, the described experiments test the viability of specific tools required for large-scale processing [6, 11], including the ability to separate ion qubits and move them to separate zones of the trap while maintaining their entanglement, manipulate and detect the qubit states without the need for strongly focussed laser beams, and perform QIP operations conditioned on the measurement outcomes of ancilla qubits.

4 Quantum simulation

As originally conjectured by Feynman [2], a universal quantum computer could efficiently simulate the dynamics of many-body quantum systems.

[1] The spectral resolution for the transition frequency in the two-level system is proportional to t^{-1}, t being the (laser) pulse length to obtain the transition. In a Ramsey experiment, one splits the one pulse into two pulses separated by a time delay T. If the pulses are coherent and this qubit (ion) does not decohere during T, the spectral resolution is increased to be proportional to T^{-1}. By increasing the relative phase difference between the two pulses, one can observe Ramsey fringes, the oscillation in the two-level system in dependence on this relative phase.

Simulations of some tens of interacting qubits could already be intractable for the most powerful classical computers. For instance, the generic state of 30 spin-$\frac{1}{2}$ particles is defined by 2^{30} numbers and to describe its evolution a matrix of $2^{30} \times 2^{30}$ has to be exponentiated [32]. Increasing classical calculation capabilities cannot help to efficiently simulate even only slightly larger quantum systems (note, for 300 particles 2^{300} numbers describe the state, close to the estimated number of protons in the universe).

On the other hand, to exceed the performance of classical computers in, for example, factorizing, one will have to control the order of 10^5 qubits. Even though there appear to be no fundamental limits in scaling up the basic processor and memory unit described in the multiplexer approach, there is still challenging technology to be developed, with a time scale probably measured in decades. Thus, to gain deeper insight into the dynamics of quantum systems, an alternative approach could be taken into consideration.

Instead of translating quantum dynamics into an algorithm to run on a universal quantum computer, one could choose a system to be controlled and manipulated with its evolution being governed by the same Hamiltonian as the system to be simulated [31]. More importantly, one could call this analog quantum simulator a quantum computer designed to address a certain set of problems in an even more efficient way than a universal quantum computer.

The Hamiltonians that can be realized with trapped ions can show a Heisenberg-like interaction [31, 32]. Quantum spin Hamiltonians of this type describe magnetism in many solid-state systems like magnets, high-T_c superconductors, quantum Hall ferromagnets, ferroelectrics, etc., and their simulation would allow one to observe and analyze quantum phase transitions [31].

As an example, we describe the quantum Ising model, and discuss how the simulation could be implemented in an ion trap. The quantum Ising Hamiltonian ($H_{\mathrm{Ising}} = J \sum_{m=n+1} \sigma_m^z \sigma_n^z + B_x \sum_m \sigma_m^x$) consists of two contributions. The first part represents the interaction between the spins of nearest neighbors in the one-dimensional spin chain, where the amplitude of J represents the interaction strength while its positive (negative) sign stands for an anti-ferromagnetic (ferromagnetic) interaction. The latter part can be understood as the interaction of a magnetic field with each spin independently.

For the ion string, the parameters can be manipulated independently. Changing the intensity of the laser beams providing the effective magnetic field B_x alters the field amplitude; changing the intensity of the beams providing the optical dipole force alters the amplitude of the interaction strength $|J|$. The sign of J can be controlled via the relative angle between the optical dipole force and the z axis defined by the ion string, i.e. the relative direction of the laser beams. The range of interaction can be tuned by the radial trapping potential.

The possibility to control the parameters of the system and to address each single lattice site turn it into a versatile system offering tools for analysis overcoming by far the possibilities in experiments on solid-state systems [31].

The implementation of the most basic protocol for the two- and three-qubit cases, respectively, could be done in the following way: (1) initialize the two- (three)-qubit ions in the motional ground state via side-band cooling and in the internal state $|\downarrow\downarrow\rangle$ ($|\downarrow\downarrow\downarrow\rangle$) via optical pumping. (2) Switch on adiabatically an effective magnetic field B_x simulated by single-qubit gates. (3) Switch on adiabatically the effective spin–spin interaction J simulated by the state-dependent optical dipole force along (perpendicular to) the trap axis. (4) Read out the average state of the qubits. Figure 5 shows the classically simulated experimental outcome of a quantum simulation with two (three) qubits versus the ratio of the magnetic field to the interaction strength (calculation done by Diego Porras).

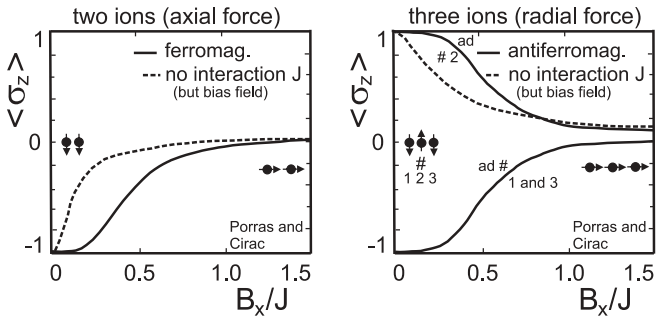

FIGURE 5 Results of the classical simulations for a quantum simulation of the quantum Ising model. The averaged spin per ion is shown versus the relative B_x/J. In the *left-hand part*, we show the expected result for a two-ion experiment. If $J > B_x$, we see a transition of the spins in a parallel ordered (ferromagnetic) phase. This is clearly distinguishable from the evolution of the spins without spin–spin interaction (but exposed to a symmetry-breaking bias field). In the *right-hand part* we see a transition into an anti-parallel (anti-ferromagnetic) order for three ions (labeled as # 1, 2, and 3. The *lower (upper) solid line* represents the average spin of the outer two (middle) ion(s)). The difference in the sign of J is caused by changing the direction of the optical dipole force from parallel to perpendicular to the trap axis

The advantages of an analog quantum simulator compared to a universal quantum computer that would simulate the interaction by executing discrete steps composed from a universal set of gates are perhaps apparent. In searching for robust effects, like quantum phase transitions, there would be no need for fault-tolerant gate operations. Also, the read out of the simulation requires only a measurement of the global fluorescence of all qubit ions.

Scaling the system to 10 qubits might already allow us to outperform classical simulations and could lead to a deeper insight into the dynamics of quantum systems. With individual addressing, we could start with a state representing a particular spin excitation. We could also analyze non-equilibrium dynamics by switching the interactions non-adiabatically.

5 Conclusions and outlook

In the last few years, the basic building blocks for a scalable architecture of a quantum information processor with trapped-ion qubits have been individually demonstrated. The experiments described here can be viewed as examples of subroutines that incorporate most of these building blocks. Sympathetic recooling [5] has been achieved separately, but must be integrated into larger computational tasks. Although it will be a non-trivial technological challenge to scale the system to many qubits, no fundamental limitations seem to exist. It also appears technically feasible to reach the fault-tolerant level for error-correction protocols with the

demonstrated one- and two-qubit gates. Therefore, trapped-ion qubits remain a promising candidate for the implementation of large-scale quantum information processing. On a shorter time scale, interesting problems might be studied by realizing an analog quantum simulator based on similar techniques, but with possibly less severe constraints on the fidelity of operations.

ACKNOWLEDGEMENTS The work described in this paper was supported by ARDA, DFG, NIST, and NSA. T. Schaetz acknowledges a Deutsche Forschungsgemeinschaft research grant. We thank D. Porras and I. Cirac for information on their proposal for analog quantum simulations.

REFERENCES

1 J.I. Cirac, P. Zoller: Phys. Rev. Lett. **74**, 4091 (1995)
2 M.A. Nielsen, I.L. Chuang: *Quantum Computation and Quantum Information*, 1st edn. (Cambridge University Press, Cambridge 2000)
3 D.J. Wineland, C.R. Monroe, W.M. Itano, D. Leibfried, B.E. King, D.M. Meekhof: J. Res. Natl. Inst. Stand. Technol. **103**, 259 (1998)
4 D. Kielpinski, C. Monroe, D.J. Wineland: Nature **417**, 709 (2002)
5 M.D. Barrett, B.L. DeMarco, T. Schaetz, D. Leibfried, J. Britton, J. Chiaverini, W.M. Itano, B.M. Jelenkovic, J.D. Jost, C. Langer, T. Rosenband, D.J. Wineland: Phys. Rev. A **68**, 042 302 (2003)
6 B.B. Blinov, L. Deslauriers, P. Lee, M.J. Madsen, R. Miller, C.R. Monroe: Phys. Rev. A **65**, 040 304 (2002)
7 J. Bollinger, D.J. Heinzen, W.M. Itano, S.L. Gilbert, D.J. Wineland: IEEE Trans. Instrum. Meas. **40**, 126 (1991)
8 R.P. Feynman, F. Vernon, R.W. Hellwarth: J. Appl. Phys. **28**, 49 (1957)
9 L. Allen, J.H. Eberly: *Optical Resonance and Two-level Atoms* (Dover, Mineola, NY 1987)
10 The laser-beam waists (approximately equal to the beam diameters) at the ions were approximately 30 μm
11 D. Kielpinski, V. Meyer, M.A. Rowe, C.A. Sackett, W.M. Itano, C.R. Monroe, D.J. Wineland: Science **291**, 1013 (2001)
12 D. Leibfried, B.L. DeMarco, V. Meyer, D. Lucas, M.D. Barrett, J. Britton, J. Chiaverini, W.M. Itano, B.M. Jelenkovic, C. Langer, T. Rosenband, D.J. Wineland: Nature **422**, 414 (2003)
13 D.J. Wineland, M.D. Barrett, J. Britton, J. Chiaverini, B.L. DeMarco, W.M. Itano, B.M. Jelenkovic, C. Langer, D. Leibfried, V. Meyer, T. Rosenband, T. Schaetz: Philos. Trans. R. Soc. Lond. A **361**, 1349 (2003)
14 The state of two qubits can be described in the Bell basis, spanned by four maximally entangled states [2]: the singlet state $|\uparrow\downarrow\rangle - |\downarrow\uparrow\rangle$ and the triplet states $|\uparrow\uparrow\rangle + |\downarrow\downarrow\rangle$, $|\uparrow\downarrow\rangle + |\downarrow\uparrow\rangle$, and $|\uparrow\uparrow\rangle - |\downarrow\downarrow\rangle$, respectively
15 D. Wineland, H. Dehmelt: Bull. Am. Phys. Soc. **20**, 637 (1975); R. Blatt, P. Zoller: Eur. J. Phys. **9**, 250 (1988)
16 http://qist.lanl.gov/
17 B.E. King, C.S. Wood, C.J. Myatt, Q.A. Turchette, D. Leibfried, W.M. Itano, C.R. Monroe, D.J. Wineland: Phys. Rev. Lett. **81**, 1525 (1998)
18 T. Schaetz, M.D. Barrett, D. Leibfried, J. Chiaverini, W.M. Itano, J.D. Jost, C. Langer, D.J. Wineland: Phys. Rev. Lett. (2004) in press
19 C.H. Bennett, S.J. Wiesner: Phys. Rev. Lett. **69**, 2881 (1992)
20 To preserve a superposition or an entangled state, no measurement that would cause the projection into some other states is allowed. A Bell-state measurement can be accomplished by transforming from the Bell basis [14] into the measurement basis, prior to the individual state measurement of each qubit. Therefore, the Bell measurement provides information about which of the four Bell states the two qubits were previously in, but no information about the states of the individual qubits. We realize this by a conditional (disentangling) phase gate followed by individual read out of the two qubits [18]
21 K. Mattle, H. Weinfurter, P.G. Kwiat, A. Zeilinger: Phys. Rev. Lett. **76**, 4656 (1996)
22 T. Schaetz et al.: submitted for publication (2004)
23 D.P. DiVincenzo: in *Scalable Quantum Computers*, ed. by S.L. Braunstein, H.-K. Lo, P. Kok (Wiley-VCH, 2001)
24 D. Leibfried, M.D. Barrett, T. Schaetz, J. Britton, J. Chiaverini, W.M. Itano, J.D. Jost, C. Langer, D.J. Wineland: Science **304**, 1476 (2004)
25 D.J. Wineland, J.J. Bollinger, W.M. Itano, F.L. Moore, D.J. Heinzen: Phys. Rev. A **46**, R6797 (1992)
26 The statistical limit is governed by quantum projection noise, arising due to the statistical nature of projecting a superposition state into one eigenstate by the measurement
27 D.M. Greenberger, M.A. Horne, A. Shimony, A. Zeilinger: Am. J. Phys. **58**, 1131 (1990)
28 M.D. Barrett, J. Chiaverini, T. Schaetz, J. Britton, W.M. Itano, J.D. Jost, E. Knill, C. Langer, D. Leibfried, R. Ozeri, D.J. Wineland: Nature **429**, 737 (2004)
29 C.H. Bennett, G. Brassard, C. Crépeau, R. Jozsa, A. Peres, W.K. Wootters: Phys. Rev. Lett. **70**, 1895 (1993)
30 H. Rohde, S.T. Gulde, C.F. Roos, P.A. Barton, D. Leibfried, J. Eschner, F. Schmidt-Kaler, R. Blatt: J. Opt. B **3**, 34 (2001)
31 D. Porras, J.I. Cirac: Phys. Rev. Lett. **92**, 207 901 (2004)
32 E. Jané, G. Vidal, W. Dür, P. Zoller, J.I. Cirac: quant-ph/0207011 (2002)
33 Q.A. Turchette, C.J. Myatt, B.E. King, C.A. Sackett, D. Kielpinski, W.M. Itano, C.R. Monroe, D.J. Wineland: Phys. Rev. A **62**, 053 807 (2000)